Monoallelic pathogenic *ALG5* variants cause atypical polycystic kidney disease and interstitial fibrosis

Graphical abstract

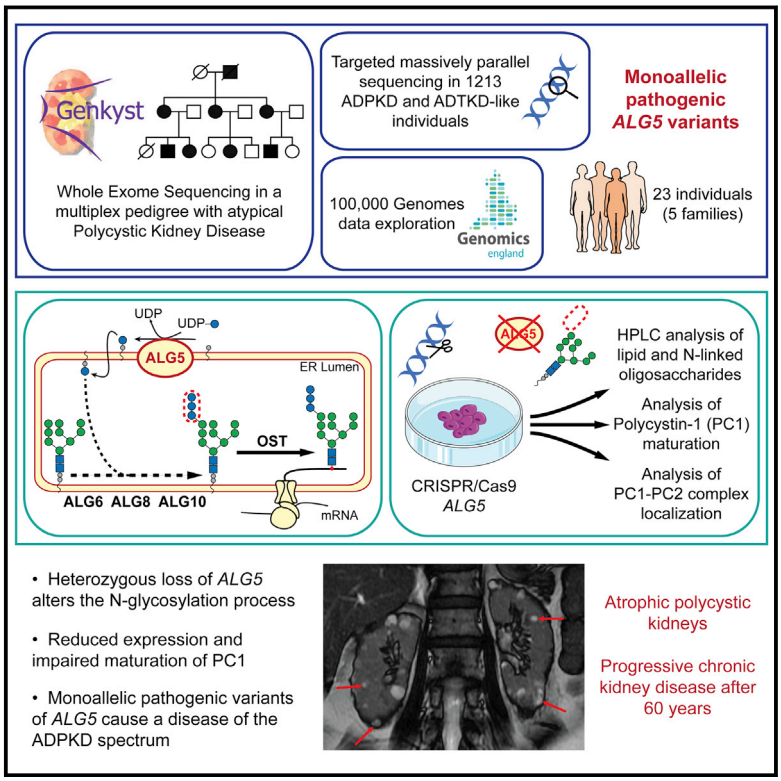

Authors

Hugo Lemoine, Loann Raud, François Foulquier, ..., Yannick Le Meur, Marie-Pierre Audrézet, Emilie Cornec-Le Gall

Correspondence

emilie.cornec-legall@chu-brest.fr

Autosomal dominant polycystic kidney disease (ADPKD) is clinically and genetically heterogeneous, with two major genes, *PKD1* and *PKD2* (encoding polycystin 1 and 2) and four minor genes. We identified monoallelic *ALG5* variants in five pedigrees affected by ADPKD-like symptoms. *ALG5* loss disrupt N-glycosylation and impacts polycystin 1 maturation and localization.

Lemoine et al., 2022, The American Journal of Human Genetics *109*, 1484–1499
August 4, 2022
https://doi.org/10.1016/j.ajhg.2022.06.013

CellPress

ARTICLE

Monoallelic pathogenic *ALG5* variants cause atypical polycystic kidney disease and interstitial fibrosis

Hugo Lemoine,[1,21] Loann Raud,[1,21] François Foulquier,[2] John A. Sayer,[3,4,5] Baptiste Lambert,[2] Eric Olinger,[3] Siriane Lefèvre,[1,6] Bertrand Knebelmann,[7] Peter C. Harris,[8] Pascal Trouvé,[1] Aurore Desprès,[9] Gabrielle Duneau,[10] Marie Matignon,[11] Anais Poyet,[12] Noémie Jourde-Chiche,[13] Dominique Guerrot,[14] Sandrine Lemoine,[15] Guillaume Seret,[16] Miguel Barroso-Gil,[3] Coralie Bingham,[17] Rodney Gilbert,[18] Genomics England Research Consortium, The Genkyst Study Group, Yannick Le Meur,[19,20] Marie-Pierre Audrézet,[1,9] and Emilie Cornec-Le Gall[1,20,*]

Summary

Disorders of the autosomal dominant polycystic kidney disease (ADPKD) spectrum are characterized by the development of kidney cysts and progressive kidney function decline. *PKD1* and *PKD2*, encoding polycystin (PC)1 and 2, are the two major genes associated with ADPKD; other genes include *IFT140*, *GANAB*, *DNAJB11*, and *ALG9*. Genetic testing remains inconclusive in ~7% of the families. We performed whole-exome sequencing in a large multiplex genetically unresolved (GUR) family affected by ADPKD-like symptoms and identified a monoallelic frameshift variant (c.703_704delCA) in *ALG5*. *ALG5* encodes an endoplasmic-reticulum-resident enzyme required for addition of glucose molecules to the assembling N-glycan precursors. To identify additional families, we screened a cohort of 1,213 families with ADPKD-like and/or autosomal-dominant tubulointerstitial kidney diseases (ADTKD), GUR (n = 137) or naive to genetic testing (n = 1,076), by targeted massively parallel sequencing, and we accessed Genomics England 100,000 Genomes Project data. Four additional families with pathogenic variants in *ALG5* were identified. Clinical presentation was consistent in the 23 affected members, with non-enlarged cystic kidneys and few or no liver cysts; 8 subjects reached end-stage kidney disease from 62 to 91 years of age. We demonstrate that *ALG5* haploinsufficiency is sufficient to alter the synthesis of the N-glycan chain in renal epithelial cells. We also show that ALG5 is required for PC1 maturation and membrane and ciliary localization and that heterozygous loss of ALG5 affects PC1 maturation. Overall, our results indicate that monoallelic variants of *ALG5* lead to a disorder of the ADPKD-spectrum characterized by multiple small kidney cysts, progressive interstitial fibrosis, and kidney function decline.

Introduction

Autosomal dominant polycystic kidney disease (ADPKD) is a systemic disorder characterized by the development of fluid-filled cysts in the kidneys, frequently associated with extra-renal manifestations such as liver cysts and intracranial aneurysms.[1] ADPKD-affected individuals represent ~3% to 6% of the incident subjects with end-stage kidney disease (ESKD) each year (see annual reports of United States Renal Data System and of the French Renal Epidemiology and Information Network (REIN) in web resources). ADPKD is predominantly caused by pathogenic variants in *PKD1* (MIM: 601313) and *PKD2* (MIM: 173910), involved in ~75% and 18% of the families, respectively.[2,3] *PKD1* and *PKD2* encode polycystin (PC)1 and PC2, which are membrane asparagine N-linked glycoproteins (N-linked glycoproteins) functionally expressed at the primary cilium.[4] PC1 is cleaved at a G protein-coupled receptor proteolytic site (GPS), and the level of mature, cleaved glycoforms of PC1 has been shown to correlate with disease severity.[5,6] In the past few years, several other genes have been associated with ADPKD-like phenotypes, including notably genes involved in the endoplasmic reticulum (ER) glycosylation machinery and/or ER folding pathway such

[1]Univ. Brest, Inserm, UMR 1078, GGB, 29200 Brest, France; [2]Univ. Lille, CNRS, UMR 8576 – UGSF - Unité de Glycobiologie Structurale et Fonctionnelle, 59000 Lille, France; [3]Translational and Clinical Research Institute, Faculty of Medical Sciences, Newcastle University, Newcastle Upon Tyne NE1 3BZ, UK; [4]The Newcastle upon Tyne Hospitals NHS Foundation Trust, Renal Services, Freeman Road, Newcastle Upon Tyne NE7 7DN, UK; [5]NIHR Newcastle Biomedical Research Centre, Newcastle University, Newcastle Upon Tyne NE4 5PL, UK; [6]Service de Néphrologie, Hôpital de Lorient, 56322 Lorient, France; [7]Service de Néphrologie et Transplantation rénale, Hôpital Necker, APHP, Université de Paris, Paris, France; [8]Division of Nephrology and Hypertension, Mayo Clinic, Rochester, MN 55902, USA; [9]Service de Génétique moléculaire, CHRU Brest, 29609 Brest, France; [10]Association des Urémiques de Bretagne, Lorient, France; [11]University Paris Est Créteil, Institut National de la Santé et de la Recherche Médicale (INSERM), Assistance Publique des Hôpitaux de Paris (AP-HP), Hôpitaux Universitaires Henri Mondor, Service de Néphrologie et Transplantation, Fédération Hospitalo-Universitaire "Innovative Therapy for Immune Disorders", Créteil, France; [12]Association Régionale d'Aide aux Urémiques du Centre Ouest (ARAUCO), Bourges, France; [13]Centre de Néphrologie et Transplantation Rénale, Hôpital de la Conception (APHM), Marseille, France; [14]Service de Néphrologie, Dialyse et Transplantation, CHU de Rouen, Rouen, France; [15]Néphrologie, Dialyse, Hypertension artérielle et Exploration Fonctionnelle rénale, Groupement Hospitalier Edouard Herriot, Hospices Civils de Lyon, Lyon, France; [16]Néphrologie-Dialyse, Association ECHO, Le Mans, France; [17]Royal Devon and Exeter NHS Foundation Trust, Exeter EX2 5DW, UK; [18]Southampton Children's Hospital, University of Southampton, Southampton SO16 6YD, UK; [19]Univ Brest, UMR 1227, LBAI, Labex IGO, 29200 Brest, France; [20]Service de Néphrologie, Hémodialyse et Transplantation rénale, CHRU Brest, 29609 Brest, France
[21]These authors contributed equally
*Correspondence: emilie.cornec-legall@chu-brest.fr
https://doi.org/10.1016/j.ajhg.2022.06.013.

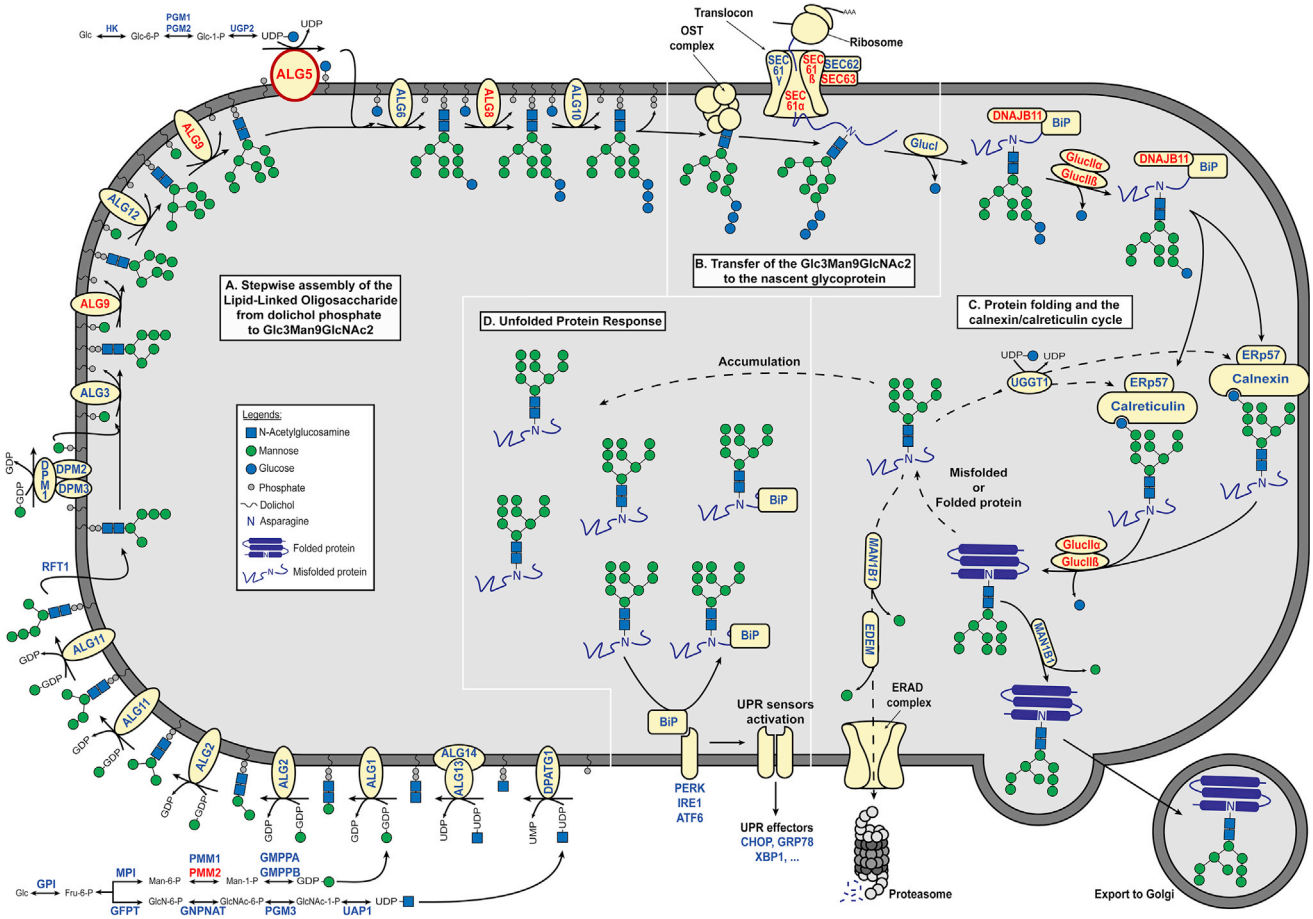

Figure 1. N-glycosylation pathway

Enzymes and other proteins associated with diseases of the ADPKD/ADPLD/ADTKD spectrum are shown in red.

(A) Stepwise assembly of the lipid-linked oligosaccharide (LLO). LLO precursors of N-glycans are initially assembled on dolichol on the cytoplasmic side of the endoplasmic reticulum (ER) membrane, and flipped into the ER, where mannose and glucose units are added to form a 14-sugar structure—Glc3Man9GlcNAc2. ALG5 catalyzes the synthesis of the donor-substrate dolichol phosphate-glucose, which provides glucose residues for transfer on the growing LLO by ALG6, ALG8, and ALG10.

(B) Transfer of the lipid-linked oligosaccharide. An oligosaccharyltransferase (OST) adds the glycan chain to a protein at an Asn (N)-X-Ser/Thr site (in which X denotes any amino acid except for proline).

(C) Protein folding and the calnexin/calreticulin cycle. Glucosidase I (GlucI) removes the outermost glucose before glucosidase II (GlucII), composed of α and β subunits, removes the second glucose. This is a prerequisite for the entry of the nascent peptide into the calnexin (CNX)/calreticulin (CRT) protein folding and quality control cycle. GlucII subsequently removes the innermost glucose from the N-linked glycan, allowing for exit from the CNX/CRT cycle and proceeding along the secretory pathway. Misfolded proteins are recognized and reglucosylated by UGGT, allowing reentry into the CNX/CRT cycle. Eventually, proteins that fail to fold properly undergo ER-associated degradation by retrotranslocation through the SEC61 translocon complex into the cytoplasmic compartment, where they are degraded by the proteasome.

(D) Unfolded protein response. An accumulation of misfolded protein in the ER lumen leads to the activation of the UPR signalization pathways through the dissociation of BiP from the UPR sensors PERK, ATF6, and IRE-1.

as *GANAB* (MIM: 104160), *DNAJB11* (MIM: 611341), *ALG8* (MIM: 617874), and *ALG9*.[2,7–11] In addition, monoallelic pathogenic variants to *IFT140,* a gene previously linked to a recessively inherited syndromic ciliopathy (MIM: 614620), were very recently shown to be associated with atypical, mild forms of polycystic kidney disease.[12] The identification of these "new" genes in atypical forms of polycystic kidney disease has highlighted the genetic overlap between clinical entities once thought to be distinct: ADPKD, autosomal-dominant polycystic liver disease (ADPLD), and autosomal-dominant tubulointerstitial disease (ADTKD), a group of nephropathies characterized by progressive tubulointerstitial fibrosis with no or few kidney cysts.[13–15] Yet, despite this recent expansion of the genetic spectrum of ADPKD and the increased awareness on differential diagnoses of cystic kidney diseases, ADPKD remains genetically unresolved in ~7% of the families.[3,12,16]

N-glycosylation is one of the main posttranslational modifications of membrane and secreted glycoproteins (Figure 1).[17] PC1 and PC2 are no exception to this rule, with 61 predicted N-glycosylation sites for PC1 and 5 for PC2.[18,19] The first steps initiating the N-linked glycosylation occurs in the ER membrane through the so-called "dolichol cycle." This cycle, operating both at the cytosolic

face and luminal face of the ER, involves numerous glycosylation enzymes, substrates, and donors for the synthesis of a specific oligosaccharide precursor linked to a dolichyl pyrophosphate (Dol-PP) carrier whose final glycan structure is Glc3Man9GlcNAc2-PP-Dol. The last step of the dolichol cycle relies on the cotranslational transfer of Glc3Man9GlcNAc2 from Glc3Man9GlcNAc2-PP-Dol onto nascent proteins in the ER lumen by the oligosaccharyltransferase (OST) complex. The OST complex can be composed of two different catalytic subunits (STT3A or STT3B) and a set of accessory subunits defining two subcomplexes with two different but complementary functions. While the STT3A complex mediates cotranslational glycosylation, STT3B complex mediates cotranslational and/or posttranslocational glycosylation of acceptor sites that have been skipped by the STT3A complex.[17] The amount and structure of the lipid-linked oligosaccharide (LLO) intermediate appears crucial for the fate of the glycoproteins as a very efficient quality control system based on the glycan structure occurs in the ER lumen. Based on the use of lectins, enzymes, and chaperones, this tight ER quality control for N-linked glycoproteins is fundamental for a given protein to acquire its own specific conformation that may trigger its fate in terms of subcellular localization, biological function, and sorting. As such, any defects in the dolichol pathway, transfer, and/or quality control will massively affect the functions of N-glycoproteins.[20]

In this study, we identified *ALG5* as a candidate gene in atypical forms of ADPKD by employing global and targeted sequencing in families with unresolved ADPKD and ADTKD. *ALG5* encodes a transmembrane-bound enzyme of the ER dolichol cycle, the dolichyl-phosphate beta-glucosyltransferase that participates in the synthesis of the Dol-P-Glc donor substrate required for the synthesis of the glucosylated LLO precursor in the ER lumen (Figure 1).[21,22] The three glucose residues added on the top of the Man9GlcNAc2-PP-Dol structure by ALG6, ALG8, and ALG10 are known to be essential for OST specificity. Variants in *ALG5* are not currently associated with any human diseases in OMIM. We show that heterozygous loss of *ALG5* is sufficient to alter both LLO and N-linked oligosaccharides (NLO) structures in renal tubular epithelial cells *in vitro* and that the loss of *ALG5* results in alteration of PC1 maturation and localization. Altogether, our data establish *ALG5* as an additional gene associated with the ADPKD spectrum. *ALG5* nephropathy is associated with non-enlarged polycystic kidneys, few or no liver cysts, and progressive loss of kidney function after the sixth decade.

Subjects and methods

Sample and data collection

A total of 1,213 individuals from ADPKD- and ADTKD-affected families were enrolled. The participants originated from ADPKD and ADTKD cohorts: the Genkyst/GeneQuest study (Clinical trials NCT02112136) (n = 170), the NTIH study (Clinical trials NCT01312727) (n = 82); and 961 unrelated individuals with ADPKD and ADPLD-like phenotypes analyzed in Brest University Hospital. While in 137 individuals (82 ADTKD, 55 ADPKD), genetic analysis of ADPKD- and ADTKD-associated genes had already been performed and had been inconclusive, 1,076 individuals did not have previous genetic testing. The relevant Institutional Review Boards or ethics committees approved all studies, and participants gave informed consent. Clinical, imaging data, and familial information were obtained by review of clinical and study records and/or during medical interviews. Kidney function was calculated from clinical serum creatinine measurements with the Chronic Kidney Disease Epidemiology Collaboration (CKD-EPI) formula.[23] Blood or saliva samples for standard DNA isolation were collected from the probands and all available family members.

Whole-exome sequencing and bioinformatics analysis

Whole-exome sequencing was performed in family PK20267. Whole-exome capture was performed with the Agilent SureSelectXT Human All Exon V6 Kit and the enriched library was sequenced with 150 bp paired-end reads on a Novaseq 6000 sequencer (Novogen HK Company Limited). FASTQ files were aligned to the hg19 reference genome (UCSC Genome Browser), and realignment and recalibration were performed with the Genome Analysis Toolkit (GATK) (3.3-0). Multi-sample variant calling was performed with the GATK (3.3-0) HaplotypeCaller, and variants were filtered with Variant Quality Score Recalibration for both SNVs and indels. Variant mining was performed with Golden Helix SNP & Variation Suite v.8 (SVS) with the following filters: (1) read depth ($\geq$10×) and genotype quality ($\geq$20), (2) selection for autosomal-dominant sample genotype pattern, (3) removal of Genome Aggregation Consortium (GnomAD) browser variants with a minor allele frequency (MAF) $>$ 0.1%, and (4) characterization of coding and non-coding SNVs within 14 bp of the splice site and subsequent removal of SNPs predicted to be neutral by $\geq$2/6 dbNSFP tools (SIFT, PolyPhen-2 HVAR, MutationTaster, Mutation Assessor, FATHMM, and FATHMM MKL). The variants that remained after the SVS analysis are listed in Table S1.

Targeted massively parallel sequencing

We developed a custom gene panel (Nimblegen, Roche) to capture the coding regions and ~50 bp flanking regions of 25 genes including 22 genes known to be associated with either ADPKD or ADPLD, or other inherited nephropathies associated with kidney cysts or with ADTKD. An update of this panel was performed during the study, with inclusion of two additional genes (*IFT140* and *ALG6*, full list available in Table S2). Genomic DNA was quantified by Qubit and 100 ng of DNA was enzymatically fragmented. Libraries were prepared using the Kapa HyperCapture kit (Roche), and 40 samples were pooled before capture. The captured libraries were sequenced using the Miniseq sequencer (Illumina) with 150 bp paired-end reads. Sequence alignment was performed employing Burrows-Wheeler Aligner (BWA) and GATK IndelRealigner, variant calling was performed using Isaac Variant Caller, and variants were subsequently annotated using Golden Helix SVS and SeqOne Genomics.

Genomics England 100,000 genomes project

All participants in the Genomics England 100,000 Genomes Project provided written consent to access their anonymized clinical and genomic data for research purposes. The project model and its informed consent process have been approved by the National Research Ethics Service, Research Ethics Committee for East of England (Cambridge South Research Ethics Committee).

Whole-genome sequencing (WGS) was performed with the Illumina TruSeq DNA PCR-Free sample preparation kit (Illumina) and an Illumina HiSeq 2500 sequencer, generating a mean depth of 45× (range from 34× to 72×) and greater than 15× for at least 95% of the reference human genome. WGS reads were aligned to the Genome Reference Consortium human genome build 38 (GRCh38) with Isaac Genome Alignment Software (v.01.14; Illumina). Sequence data were analyzed with bcftools scripts designed to search vcf.gz files, and individual BAM files were viewed with IGV. Variant annotation was performed with Ensembl Variant Effect Predictor (VEP). Phenotypes of identified individuals harboring *ALG5* likely pathogenic variants were manually reviewed in Genomics England Participant Explorer. We reviewed tiering data, exomiser data, and exit questionnaires (Main programme_V13_2021-09-30), filled in by the clinicians at the NHS Genomics Medical Centres (GMCs) for each case, to exclude other genes associated with inherited kidney diseases. Those recruited under rare primarily kidney disorders included 3,520 probands, and those recruited under the "normalized specific disease" term cystic kidney disease included 1,546 individuals including 1,289 family probands.

Using CRISPR-Cas9 to generate *ALG5*-mutated cell lines

CRISPR-Cas9 targeting of *ALG5* was performed in human renal cortical tubular epithelial (RCTE) cells. Briefly, a pair of gRNAs, targeting exons 2 and 8 with the strongest predictive scores (http://crispor.tefor.net), were cloned into pSpCas9(BB)-2A-GFP (PX458, Addgene plasmid # 48138) and verified by sequencing. The pair of gRNAs was then transiently transfected in wild-type RCTE cells by electroporation using the A-020 program of the Amaxa Nucleofector II (Lonza) following the manufacturer's instructions. After 48 h, single-cell clone selection of GFP-high-positive cells was then isolated in a 96-well plate by cell sorting (Moflo XDP, Beckman Coulter). Cells were grown for 14 days and re-seeded for screening performed with genomic DNA extraction followed by amplification using screening primers set and Sanger sequencing. Selected clones were additionally screened by RT-qPCR and Western blotting. *ALG5*-null and heterozygous clones were selected for the functional characterization of *ALG5* loss. Targeted sequencing of the 27 genes listed in Table S2 was performed for all the clones employed in the study to confirm the absence of off-target variants.

Metabolic and pulse radiolabeling

RCTE cells were preincubated in DMEM containing 10% of dialyzed Fetal Bovine Serum (Corning, USA) and 0.5 mM of glucose before being metabolically labelled with [2-3H] mannose (PerkinElmer). When used, RCTE cells were preincubated and incubated with castanospermine at the final concentration of 50 μg/mL. After metabolic labelling, cells were washed three times with 1× D-PBS and sequential extraction and purification of oligosaccharide material were performed as described previously.[24] Analysis of the oligosaccharide samples was performed by high-performance liquid chromatography (HPLC) using an amino-derived Asahipak NH2P-50 4E column (250 × 4.6 mm; Shodex-Showa Denko K.K [SDK]).

Plasmids production and transfection

The whole *ALG5* open reading frame (ORF) including the stop codon (GenBank: NM_013338.5) was subcloned into pCMV6-Entry Mammalian Expression Vector (CAT#: PS100001, Origene) using BamHI and MluI restriction enzymes by homologous recombination using In-Fusion HD Cloning Kit (Clontech) following the manufacturer's recommendation. Variants of interest were generated by site-directed mutagenesis using QuikChange Lightning Site-Directed Mutagenesis Kit (Agilent Technologies) following the supplier instructions. Direct sequencing was performed for sequence confirmation of the variant pALG5 vectors. mCherry-hPC1 and GFP-hPC2 constructs used in this study have been previously described.[6] RCTE cells were split 1:2 the day before electroporation and transfected at approximately 80% confluency. Transfection was performed, with 1 μg of each plasmid, using the A-020 program of the Amaxa Nucleofector II (Lonza) following the manufacturer's instructions. Stable mCherry-hPC1 cells were recovered at 33°C overnight to promote folding and expression of the tagged protein, then washed and returned to 37°C. Stable mCherry-hPC1 expression was achieved by growing cells for 4 days after transfection in cell culture media supplemented with 900 μg/mL of G418 (Invitrogen).

Western blot studies and glycosylation analysis

Cells were grown to ∼95% of confluence, washed with ice-cold DPBS, and scrapped and crude membrane protein was extracted as previously described.[6,9,11] For deglycosylation assay, crude membrane proteins were treated with 1,000 units of EndoH or 500 units of PNGaseF according to the manufacturer's (New England BioLabs) instructions and subjected to SDS-PAGE. For immunoblot, 80 μg of crude membrane protein was denatured in 1× Laemmli Sample Buffer at 65°C for 10 min. PVDF membranes were blocked 1 h in 5% nonfat milk in Tris-buffered saline plus 0.1% Tween-20 and exposed to PC1-NT antibody overnight at 4°C. Next, the HRP-conjugated secondary antibody was added for 2 h at room temperature. Protein ratio of NTR/NTS and PC1 protein level was calculated following ImageJ densitometric analysis.

Immunofluorescence, surface labeling of PC1, and ciliary localization of PC2

Transfected RCTE cells were grown on glass coverslips for 16 h then cooled at 4°C for 15 min, washed once in ice-cold PBS, and prechilled mCherry antibody diluted in IF buffer (1% BSA, 0.1% Tween-20, and PBS [pH 7.5]) was added for 45 min at 4°C. Cells were then fixed in 4% PFA (15 min at 4°C followed by 5 min at RT) and AF647-conjugated secondary antibody was added in IF buffer for 30 min in the dark. For ciliary localization of PC2, coverslips were fixed with 4% PFA for 10 min at room temperature and then washed twice with DPBS, permeabilized with 0.1% Triton X-100 for 10 min, and blocked with IF buffer. Immunofluorescence staining was done with anti-ARL13B and anti-PC2 antibodies for 1 h at room temperature. After several washes, cells were then incubated with AF488 and AF647-conjugated secondary antibodies for 1 h in the dark and then washed three times with 0.1% Tween-20 in PBS (pH 7.5). All coverslips were mounted in an antifade solution containing DAPI and fluorescence microscopy was performed using an Axio Imager M2 microscope (Zeiss).

Unfolded-protein response assay

RCTE cell lines were seeded in a 6-well plate the day before treatment with 10 mM of DTT (Invitrogen) to induce the UPR or vehicle for 2 h. Total RNA was extracted (Nucleospin RNA plus, Macherey-Nagel) and one microgram of total RNA served as a template for reverse transcription (SuperScript IV Reverse Transcriptase, Invitrogen) according to the manufacturer's instructions. Next, the neosynthesized cDNA (1 μL of a 1:10 dilution) was mixed with 2× ONEGreen Fast qPCR Premix (Ozyme) and 10 μM of the specific primers in a 10 μL

final volume. Real-time PCR was performed on the LightCycler II 480 (Roche). For immunoblot, cells were grown to ~80% of confluence and treated with Thapsigargin 0.5 μM for 4 h or DTT 10 mM for 2 h. Cells were then washed with ice-cold DPBS, trypsinized and reconstituted in RIPA buffer with protease inhibitors, incubated on ice for 30 min, and vortexed regularly. Homogenized whole lysates were centrifugated at 15,000 RPM for 15 min. 100 μg of whole lysates protein was denatured in 1× Laemmli Sample Buffer at 95°C for 5 min. PVDF membranes were blocked for 1 h in 5% non-fat milk in PBS plus 0.1% Tween-20 and exposed to primary antibodies overnight at 4°C and HRP-conjugated secondary antibodies were added for 2 h at room temperature.

Antibodies

The following antibodies were used in western blot and immunofluorescence analyses: ALG5 (rabbit pAb, Cat.#PA5-109380, Invitrogen; 1/500 for WB), PC1-NT (N-terminal, 7e12 mouse mAb, Cat.#sc-130554, Santa Cruz; 1/1,000 for WB), PC2 (YCE2 mouse mAb, Cat.#sc-47734, Santa Cruz; 1/1,000 for WB and 1/250 for IF), EGFR (A-10 mouse mAb, Cat.#sc-373746, Santa Cruz; 1/1,000 for WB), XBP1s (D2C1F rabbit mAb, Cat.#12782, Cell Signaling; 1/1,000 for WB), GADD153/CHOP (L63F7 mouse mAb, Cat.#2895, Cell Signaling; 1/1,000 for WB), IRE1α (14C10 rabbit mAb, Cat.#3294, Cell Signaling; 1/1,000 for WB), GRP78/HSPA5 (rabbit pAb, Cat.#NBP1-06274SS, Novus; 1/2,000 for WB), anti-β-Actin-HRP (C4, Cat.#sc-47778-HRP, Santa Cruz; 1/20,000 for WB), anti-mouse-IgG-HRP (Cat.#G-21040, Invitrogen; 1/10,000 for WB), anti-rabbit-IgG-HRP (Cat.#A0545, Sigma-Aldrich; 1/20,000 for WB), mCherry (rabbit pAb, Cat.#5993-100, BioVision; 1/1000 for IF), Acetyl-alpha Tubulin (6-11B-1 mouse mAb, Cat.#32-2700, Invitrogen; 1/500 for IF), ARL13B (rabbit pAb, Cat.#17711-1-AP, Proteintech, 1/500 for IF), anti-Rabbit Alexa Fluor 647 (Cat.#A32733TR, Invitrogen; 1/1,000 for IF), anti-Mouse Alexa Fluor 488 (Cat.#A32766TR, Invitrogen; 1/1,000 for IF).

Results

WES identifies *ALG5* as a promising candidate in a family with genetically unresolved ADPKD-like phenotype

In individual II.7 from family PK20267 (Figure 2), a diagnosis of ADPKD was made at 37 years of age by abdominal ultrasound (US), performed in the context of a familial history of kidney disease. At 52 years, her kidney function was preserved (eGFR 86 mL/min/1.73 m^2), she had hypertension, and a renin-angiotensin system (RAS) inhibitor was introduced. Abdominal magnetic resonance imaging (MRI) showed non-enlarged polycystic kidneys and 2 mm-sized liver cysts (Figure 2, Table 1). At 56 years her eGFR was 66 mL/min/1.73 m^2. Her father had died at 49 years of age from metastatic cancer without a diagnosis of CKD, while her three paternal half-sisters, individuals II.1, II.3, and II.5, had all reached ESKD at the respective ages of 69, 68, and 62 years. The three sisters all presented with atrophic polycystic kidneys and few or no liver cysts on computerized tomography (CT)-scans (Figures 2B and 2C). Individual II.3 underwent a nephrectomy of the left kidney after reaching ESKD, and histological examination revealed significant and widespread interstitial fibrosis in the non-cystic parenchyma; no specific lesion was observed in the non-sclerotic glomeruli (Figure S1). Of interest, severe colonic diverticulosis was reported in the four siblings (Table 1). Individual III.6, the daughter of II.3, was also found to have multiple bilateral kidney cysts and had normal kidney function at the age of 45 years (Figure 2F). Because no pathogenic variant had been identified in *PKD1, PKD2, HNF1B, DNAJB11,* or *GANAB* in II.7, WES was performed in the proband and her four affected relatives II.1, II.3, II.5, and III.6. WES analysis led to the identification of an *ALG5* variant as the most promising candidate (Table S1). *ALG5* (in chromosomal region 13q13.3; genomic size 50.5 kb) has two isoforms both ubiquitously expressed. We employed isoform 1 (GenBank: NM_013338.5, 324 amino acids, 37 KDa, 10 exons and 975 bp of coding sequence), which is the larger splice product and which is more abundantly expressed in kidney tissue, for mutation screening and designation. The frameshifting *ALG5* variant identified, c.703_704delCA (p.Gln235Valfs*21), was confirmed by Sanger sequencing. Data from the Genome aggregation database (GnomAD; 125,748 exomes and 15,708 genomes) indicate that *ALG5* is depleted in predicted loss-of-function (pLoF) variants, with a constraint score (pLoF observed/expected) of 0.22 (0.9 CI: 0.11–0.45), compatible with an intolerance to pLoF and a haploinsufficiency mechanism.[25] The extended co-segregation analysis confirmed the absence of the *ALG5* variant in individuals III.5, III.7, and III.9 who had no cysts by abdominal US, had normal kidney function, and were all between 45 and 50 years old. The *ALG5* pathogenic variant was identified in individuals III.3, III.4, III.8, and III.11. All of them had preserved kidney function, and while multiple millimeter-sized kidney cysts were identified in III.4 at 54 years and III.8 at 50 years, MRI showed only one microcyst in the left kidney of 30-year-old individual III.11.

Identification of additional families with predicted pathogenic *ALG5* variants in ADPKD/ADTKD cohorts

Analysis of 1,213 individuals with ADPKD-like, ADPLD-like, or ADTKD-like phenotypes by targeted massively parallel sequencing led to the identification of two additional families with *ALG5* segregating predicted pathogenic variants. Details about the results of this genetic screen are included in Figure S2. In family 2 (Figure 3A), female individual III.3 was incidentally diagnosed with CKD stage 3 and atrophic polycystic kidneys at 60 years and reached ESKD at 78 years of age. Her sister III.1 had an eGFR of 20 mL/min/1.73 m^2 at 85 years of age and had atrophic kidneys with multiple small kidney cysts (Figure 3E). Their mother and maternal grandmother were also presumably affected by the same disease: individual II.3 had died shortly after the initiation of peritoneal dialysis at 90 years and had atrophic polycystic kidneys, while individual I.1's reported cause of death was uremia at 90 years of age. A heterozygous nonsense variant of *ALG5* exon 8, c.773G>A (p.Trp258*), was identified in III.1 and III.3. This variant was subsequently identified in three other family members. Individual IV.1, the son of III.1, had

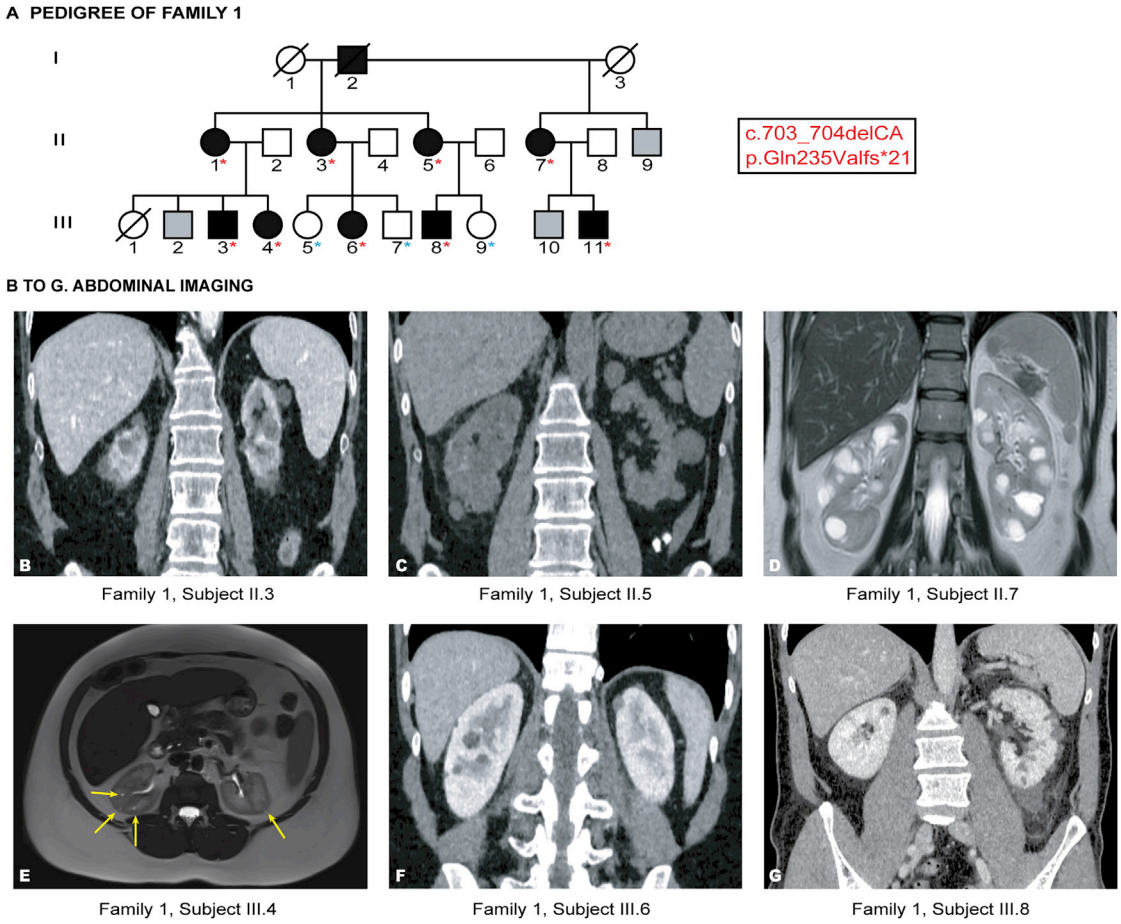

Figure 2. WES analysis reveals *ALG5* c.703_704delCA in family 1 as the likely pathogenic variant

(A) Pedigree of family 1 (PK20267) black squares or circles indicate affected male or female subjects, respectively, presenting with bilateral kidney cysts, kidney failure, and/or genetically diagnosed, and gray symbols indicate subjects where clinical information is unavailable. Clinical characteristics are detailed in Table 1. Red or blue asterisks, respectively, indicate presence or absence of the c.703_704delCA (p.Gln235Valfs*21) *ALG5* variant.

(B–G) Abdominal imaging of six affected members of family 1. Four had computed tomography (CT), with contrast-enhanced CT for II.3, III.6, and III.8 (B, F, G) and non-enhanced CT in II.5 (C). Two individuals had magnetic resonance imaging (MRI): subjects II.7 (D) and III.4 (E, yellow arrows indicate microcysts).

bilateral small kidney cysts visible on MRI and an eGFR of 59 mL/min/1.73 m^2 at 63 years (Table 1, Figure 3F), while individual IV.4 had an eGFR of 96 mL/min/1.73 m^2 at 55 years and bilateral kidney cysts (Figure 3G). Individual IV.6 had an eGFR of 53 mL/min/1.73 m^2 at 52 years and multiple small bilateral kidney cysts on MRI (Figure 3H). In family 3 (Figure 3B), the diagnosis of polycystic kidney disease was made simultaneously in the proband and her brother, at 64 and 65 years, following abdominal imaging performed in the context of abdominal pain. Both siblings had multiple kidney cysts in normal-sized kidneys (Figures 3I–3J). Their father had reached ESKD at 68 years; he had atrophic kidneys with multiple small kidney cysts. The *ALG5* variant c.635G>A (p.Arg212His) was identified in both siblings. This conservative change affects an invariant residue (Figure 3D), is absent from GnomAD database, and is predicted to be damaging with a Phred-scaled Combined Annotation Dependent Depletion (CADD) score of 33.

Identification of additional individuals with predicted pathogenic *ALG5* variants in the Genomics England 100,000 genomes project

The Genomics England 100,000 Genomes Project data were analyzed for monoallelic rare and predicted pathogenic variants in *ALG5*. As of January 2022, whole-genome sequencing was performed in 35,372 probands affected by rare diseases, including 3,520 probands with various renal and urinary tracts disorders (see details in Table S3). Pathogenic variants (truncating or otherwise described) of *ALG5* were searched for in the participants with renal disorders and identified in two probands in the cystic kidney disease subgroup (Table 2). A deletion affecting exon 1 splice site (c.54_66+1del), inherited from her mother, was identified in a 20-year-old female individual who had multiple kidney cysts, bilateral nephrocalcinosis, hypercalciuria, and a preserved kidney function. Clinical information about the mother of the proband was unfortunately missing. In a second family (Figure 3C), the variant p.Arg208His

Table 1. Clinical presentation and pathogenic variants in the 19 affected individuals from the 3 *ALG5*-affected families

Subject	Sex	eGFR[a] (age) or ESKD (age)	Context of diagnosis (age)	HBP (age)[b]	Morphology of the kidneys					Liver cysts (number)	Other significant conditions (age)
					Type	Age	Description of the cysts	Kidney length[c]	Figure		
Family 1, PK20267; c.703_704delCA (p.Gln235Valfs*21)											
II.1	F	ESKD (69)	CKD stage 3 (62)	yes (70)	CT	71[d]	atrophic kidneys with multiple small kidney cysts	R 65 L 75	N/A	no	Crohn disease; colonic diverticulosis (72)
II.3	F	ESKD (68)	incidental (64)	yes (52)	CT	70[d]	atrophic kidneys with multiple small kidney cysts	R 95 L 110	2B	yes (<10)	surgical colonic diverticulosis (63)
II.5	F	ESKD (62)	incidental (45)	yes (<35)	CT	69[d]	atrophic kidneys with multiple small kidney cysts	R 60 L 60	2C	yes (<10)	ischemic stroke (54); colonic diverticulosis
II.7	F	66 (56)	familial study (37)	yes (52)	MRI	55	normal-sized kidneys with multiple kidney cysts (largest 35 mm)	R 100 L 117	2D	yes (2)	colonic diverticulosis (52)
III.3	M	110 (52)	familial study (52)	yes (52)	N/A	N/A	N/A	–	N/A	no	elevated liver enzymes
III.4	F	100 (54)	familial study (55)	no (55)	MRI	53	normal-sized kidneys with multiple small kidney cysts	R 95 L 100	2E	no	none
III.6	F	89 (49)	incidental (47)	no (50)	CT	48	normal-sized kidneys with multiple small kidney cysts	R 110 L 100	2F	yes (2)	surgical colonic diverticulosis (49); kidney stone and nephrocalcinosis (15)
III.8	M	107 (50)	pyelonephritis (50)	no (50)	CT	50	multiple bilateral kidney cysts predominating in the right kidney	R 120 L 125	2G	no	none
III.11	M	110 (30)	familial study (30)	no (30)	MRI	30	one microcyst in the left kidney	R 105 L 110	N/A	no	none
Family 2, PK13924; c.773G>A (p.Trp258*)											
I.1[e]	F	ESKD (91)	ESKD	N/A	N/A	N/A	N/A	N/A	N/A	N/A	death of ESKD
II.3[e]	F	ESKD (90)	CKD stage 4 (85)	no (90)	US	89	atrophic kidneys with multiple small kidney cysts	N/A	N/A	N/A	atrioventricular block (87); tuberculosis
III.1	F	20 (85)	microhematuria (50)	yes (60)	US	85	atrophic kidneys with multiple small kidney cysts	R 80 L 90	3E	no	DMT2 (60); colonic diverticulosis; primary hyperparathyroidism
III.3	F	ESKD (78)	CKD stage 3 (60)	no (78)	US	71	atrophic kidneys with multiple small kidney cysts	R 98 L 86	N/A	no	gout (78)
IV.1	M	59 (63)	CKD stage 3a (64)	no (64)	MRI	62	normal-sized kidneys with 5-10 small kidney cysts per kidney	R 102 L 110	3F	no	colonic diverticulosis – segmental colectomy (57); prostate cancer (62); polycythemia (62)
IV.4	M	96 (55)	familial study (55)	no (55)	N/A	55	Normal-sized kidneys with 3-6 microcysts per kidney	R 111 L 113	3G	yes	severe osteoporosis, hearing loss

(*Continued on next page*)

Table 1. *Continued*

Subject	Sex	eGFR[a] (age) or ESKD (age)	Context of diagnosis (age)	HBP (age)[b]	Morphology of the kidneys					Liver cysts (number)	Other significant conditions (age)
					Type	Age	Description of the cysts	Kidney length[c]	Figure		
IV.6	M	53 (52)	familial study (52)	no (52)	MRI	52	Normal-sized kidneys with multiple small kidney cysts	R 107 L 106	3H	no	Hirschprung's disease, surgery in infancy
Family 3, PK14384; c.635G>A (p.Arg212His)											
I.1[e]	M	ESKD (76)	CKD stage 4 (71)	yes (71)	CT	71	atrophic kidneys with multiple small kidney cysts	R 100 L 95	N/A	no	arteritis (74), ischemic cardiomyopathy (75), subarachnoid hemorrhage (40), gout (70)
II.1	M	42 (66)	abdominal pain	yes (55)	US	66	normal-sized kidneys with multiple small kidney cysts	R 117 L 116	3I	yes (5)	none
II.2	F	60 (64)	abdominal pain	yes (50)	MRI	65	normal-sized kidneys with multiple small kidney cysts	R 100 L 110	3J	no	none

eGFR, estimated glomerular filtration rate; CKD, chronic kidney disease; CT, computed tomography; DMT2, diabetes mellitus type 2; ESKD, end stage kidney disease; HBP, high blood pressure; MRI, magnetic resonance imaging; US ultrasound imaging.
[a]Expressed as mL/min/1.73 m^2 on the basis of the last data available (CKD-EPI formula).
[b]Age at HBP diagnosis or blood-pressure measurement.
[c]R, right kidney; L, left kidney.
[d]Imaging performed after ESKD.
[e]A sample was unavailable, and so the *ALG5* variant was not confirmed.

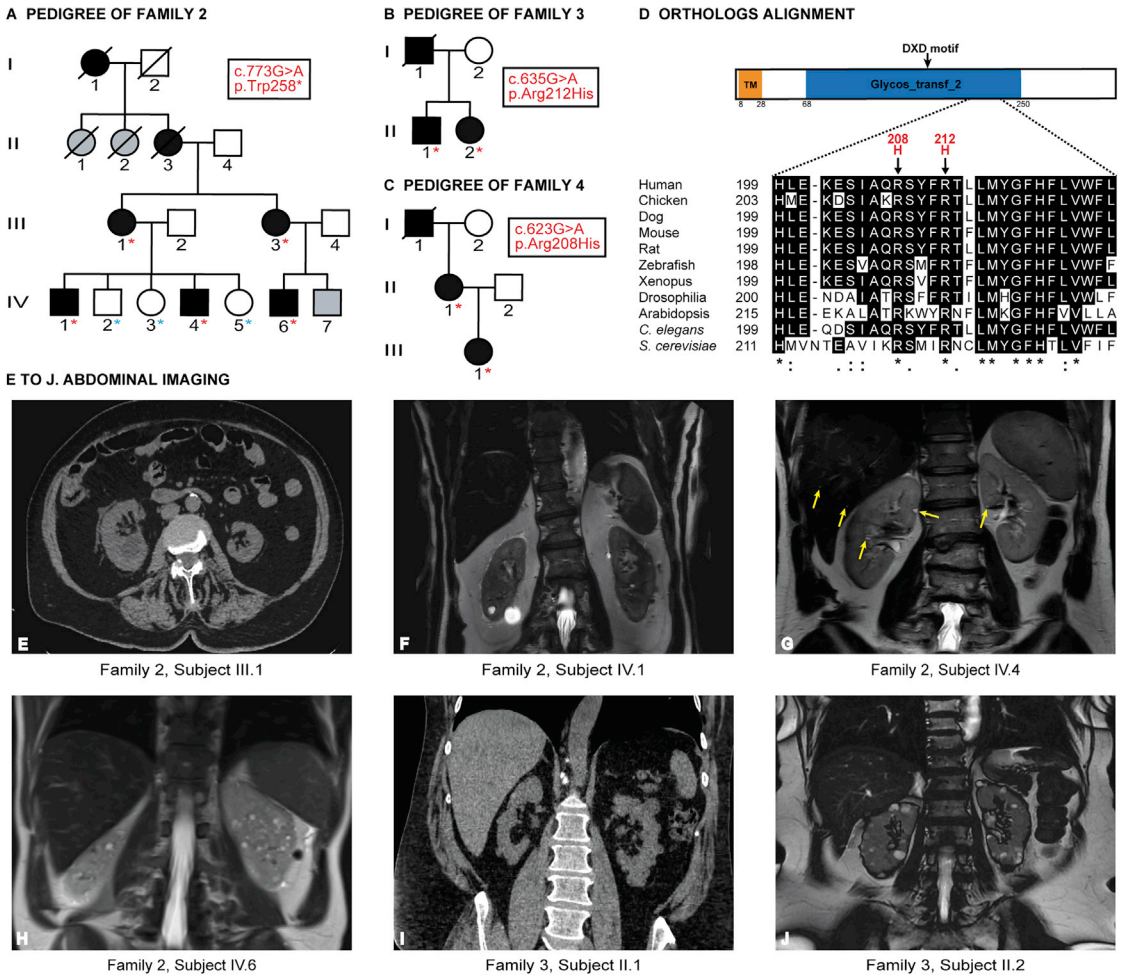

Figure 3. Identification of pathogenic variants of *ALG5* in three additional families with atypical forms of ADPKD
(A) Pedigree of family 2 (PK13924) shows 7 affected individuals. Clinical information is available in Table 1. Red or blue asterisks, respectively, indicate presence or absence of the *ALG5* c.773G>A (p.Trp258*) nonsense variant in exon 8.
(B) Pedigree of family 3 (PK14384). The *ALG5* c.635G>A (p.Arg212His) missense variant in exon 8 was identified in affected individuals II.1 and II.2. Clinical information is available in Table 1.
(C) Pedigree of family 4 (100,000 Genomes). The *ALG5* c.623G>A (p.Arg208His) missense variant in exon 8 was identified in affected individuals II.1 and III.1. Clinical information is available in Table 2.
(D) Multiple sequence alignment of *ALG5* orthologs shows invariant conservation of Arg208 and Arg212 across species. Asterisk (*), colon (:), and period (.) indicate a site with perfect alignment, belonging to a group exhibiting strong similarity, and belonging to a group exhibiting weak similarity, respectively.
(E–J) Abdominal imaging of six affected members of families 2, 3, and 4. Two individuals had non-enhanced computed tomography (CT): subjects III.1 from family 2 and II.1 from family 3 (E, I). Four individuals had magnetic resonance imaging (MRI): subjects IV.1, IV.4, and IV.6 from family 2 (F–H) and subject II.2 from family 3 (J).

(c.623G>A) was identified in a 50-year-old female participant who had multiple bilateral kidney cysts and an eGFR of 83 mL/min/1.73 m^2. Her mother had bilateral kidney cysts and atrophic kidneys, with an eGFR of 38 mL/min/1.73 m^2 at 73 years of age, and her maternal grandfather had died from ESKD. The presence of the *ALG5* variant was confirmed in her mother by Sanger sequencing. This conservative change affects an invariant residue (Figure 3D), is reported in only 1/137,447 individuals in the GnomAD database, is predicted pathogenic by 5/6 *in silico* algorithms, and has a CADD score of 33. No other variants of interest, likely to explain the nephropathy, were identified in this individual. Both families were previously considered unsolved by the Genomics England analysis after WGS and data analysis using cystic renal disease virtual panels.

ALG5 loss disturbs the assembly of the lipid-linked core oligosaccharide in human kidney epithelial cells

ALG5 plays a key role in the synthesis of the core oligosaccharide Glc3Man9GlcNAc2-PP-Dol before its transfer to selected asparagine residues of newly synthesized glycoproteins (Figure 1). We hypothesized that the ADPKD-like phenotype observed in the five families of individuals harboring *ALG5* pathogenic variants might result from a glycosylation defect leading to an impaired maturation of proteins, including notably PC1. To tackle this point, CRISPR-Cas9 targeting of *ALG5* in human RCTE cells

Table 2. *ALG5*-affected families identified in the Genomics England 100,000-genome database

Subject	Sex	eGFR[a] (age) or ESKD (age)	Aspect of the kidneys	Other significant conditions (age)
Family 4; c.623G>A (p.Arg208His)				
I.1[b]	M	ESKD (85)	N/A	cause of death: uremia
II.1	F	38 (73)	atrophic multicystic kidneys	DMT2
III.1	F	83 (50)	normal-sized kidneys with multiple cysts	HBP (41) diaphragmatic hernia
Singleton, c.54_66+1del				
N/A	F	>90 (20)	multiple kidney cysts	nephrocalcinosis, hypercalciuria

ALG5 transcript GenBank: NM_013338.5. M,male; F, female; eGFR, estimated glomerular filtration rate; ESKD, end-stage kidney disease; DMT2 diabetes mellitus type 2; HBP, high blood pressure.
[a]Expressed as mL/min/1.73 m^2 on the basis of the last data available (CKD-EPI formula).
[b]A sample was unavailable, and so the *ALG5* variant was not confirmed.

generated clones with bi-allelic frameshift mutations (null; clone AE7) or a single frameshift deletion (heterozygous; AD8 and AD9) (Table S4). The nature of the lipid-linked oligosaccharides (LLO) and N-linked oligosaccharides (NLO) in WT, AE7, and AD9 clones was investigated using HPLC after [2-3H]-mannose pulse metabolic labeling experiments (Figure 4). The highest peak classically observed in LLO profile of control cell lines corresponds to the fully assembled oligosaccharide precursor Glc3Man9GlcNAc2-PP-Dol (G3M9).[24] This structure was surprisingly not detected in WT RCTE cells where intermediate precursors corresponding to Man3-5GlcNAc2-PP-Dol (M2-M5) structures were found to accumulate (Figure 4A). NLO profile of RCTE WT cells also differed from what is normally detected in other cell lines, with several peaks representing the structures Man4 to Man9GlcNAc2 (Figure 4D). However, reanalysis of the NLO profile after treatment with castanospermine (CST), a known inhibitor of ER glucosidase I and II, resulted in the detection of glycosylated Man9 species and the loss of the structures previously observed in the absence of CST (Figure 4G). In aggregate, the atypical LLO and NLO profiles observed in WT RCTE likely result from (1) a rapid transfer of Glc3Man9GlcNac2 species from LLO to proteins and (2) a very efficient trimming of NLO species in RCTE WT cells. In *ALG5*-deficient cells, the LLO profile clearly revealed the presence of an incomplete precursor corresponding to Man9GlcNAc2-PP-Dol (M9). Although this precursor was absent in WT cells, the observed Man9GlcNAc2-PP-Dol accumulation was more pronounced in $ALG5^{-/-}$ than $ALG5^{-/+}$ cells (Figures 4A–4C). Furthermore, NLO analysis showed an accumulation of Man8GlcNAc2, Man9GlcNAc2, and Glc1Man9GlcNAc2 in *ALG5*-deficient clones (Figures 4E and 4F), arguing for a much slower maturation compared to WT RCTE cells. Interestingly, unlike in WT RCTE cells, the CST treatment did not reveal the presence of Glc32Man9GlcNAc2 species demonstrating the transfer of incomplete oligosaccharide structures. Altogether, these results highlight that *ALG5* deficiency, whether heterozygous or homozygous, leads to the accumulation of abnormal Man9GlcNAc2 LLO precursors and their transfer onto proteins in human kidney epithelial cells.

Effect of *ALG5* loss on PC1 and PC2 abundance, maturation, localization and UPR activation

We then investigated whether the lack of glycosylation was associated with an impaired maturation of PC1. Full-length PC1 undergoes autoproteolytic cleavage at the G protein-coupled proteolytic site (GPS) into a ~3,000 amino acids (aa) N-terminal fragment (PC1-NT) and a ~1,300 aa C-terminal fragment (PC1-CT) that remain associated. In WT RCTE cells, detection of PC1 with a PC1-NT antibody showed, as previously described, two different glycoforms: the mature, cell-surface-localized, EndoH-resistant PC1-NTR and the immature, intracellular, EndoH-sensitive PC1-NTS (Figure 5A).[4] Human RCTE cells contain another smaller product, Trunc_PC1, corresponding to the protein product of abnormal differential splicing across introns 21 and 22 of *PKD1* (Figure 5A).[26] In $ALG5^{-/-}$ cells, PC1-NTR was absent, while in the $ALG5^{-/+}$ cells it was less abundant by ~50% compared to WT cells (Figures 5B and 5C). Furthermore, electrophoretic migration of PC1-NTS was markedly faster in $ALG5^{-/-}$ cells, likely because of complete loss of glycosylation of PC1 in the absence of *ALG5* (Figure 5B). It is important to note that there was no difference in *PKD1* transcript expression between WT, $ALG5^{-/+}$, and $ALG5^{-/-}$ cells (data not shown), indicating that differences in steady-state protein level are translational and/or posttranslational. PC2 protein level was slightly increased in $ALG5^{-/+}$ and $ALG5^{-/-}$, as compared to WT RCTE cells (Figure 5B). No difference in PC2 migration between WT, $ALG5^{-/+}$, and $ALG5^{-/-}$ RCTE cells was observed, arguing for the absence of PC2 glycosylation defect, although it should be noted that only the ER-resident, immature version of the protein is likely seen with this whole membrane analysis, and not the mature, ciliary glycoform.[6,27] While PC1 protein level and maturation were rescued in $ALG5^{-/-}$ cells by the transfection of a wild-type *ALG5* construct, identified *ALG5* missense variants (p.Arg208His and p.Arg212His) failed to rescue PC1 maturation (Figure 5D). These findings indicate that ALG5 plays a major role in PC1 maturation. To

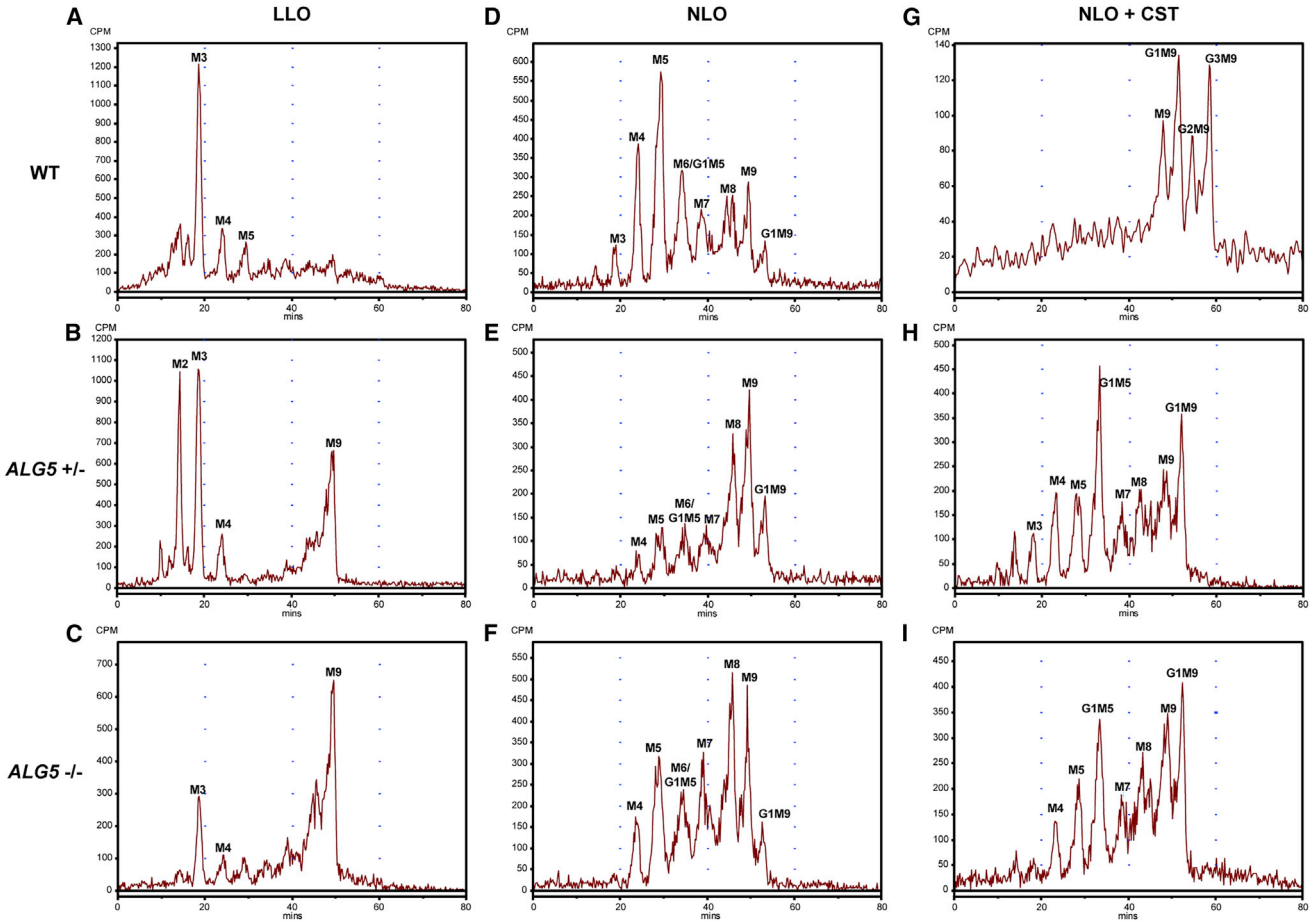

Figure 4. ***ALG5*** **loss disturbs the assembly of the lipid-linked oligosaccharides in human kidney epithelial cells**
(A–C) Lipid-linked oligosaccharides (LLO) high-performance liquid chromatography (HPLC) analysis in WT RCTE cells, *ALG5*$^{+/-}$ and *ALG5*$^{-/-}$ RCTE cells after 1 h of radioactivity labelling with [2-^{3}H] Mannose.
(D–F) Asparagine N-linked oligosaccharides (NLO) HPLC analysis in WT RCTE cells, *ALG5*$^{+/-}$ and *ALG5*$^{-/-}$ RCTE cells after 1 h of radioactivity labelling with [2-^{3}H] mannose.
(G-I) NLO HPLC analysis in castanospermin (CST)-treated WT RCTE cells, *ALG5*$^{+/-}$ and *ALG5*$^{-/-}$ RCTE cells after 1 h of radioactivity labelling with [2-^{3}H] mannose. G1-3M9 indicates oligosaccharides possessing 1 to 3 glucose (Glc), 9 mannose (Man), and 2 N-acetyl glucosamine (GlcNAc) residues. M9-M5 indicates oligosaccharides with 5 to 9 Man residues and 2 GlcNAc residues.

determine the effect of *ALG5* loss on PC1 localization by immunofluorescence, we co-transfected WT and *ALG5*$^{-/-}$ cells with tagged PC1 and PC2 constructs (Figures 5E and 5F). We observed the absence of PC1 membrane localization in PC1-PC2 co-transfected *ALG5*$^{-/-}$ cells. As PC1 and PC2 interdependence for cilia localization has been established, we analyzed PC2 to assess localization of the polycystin complex to the cilia.[6] Ciliary localization of endogenous PC2 was completely abolished in *ALG5*$^{-/-}$ cells (Figure 5G), while cilia length was not altered (Figure S3). These data indicate that ALG5 reduction affects PC1 maturation and trafficking. We finally investigated whether the accumulation of immature proteins in the ER caused by *ALG5* loss was associated with activation of the unfolded protein response (UPR). *ALG5*$^{-/-}$ and/or *ALG5*$^{-/+}$ cells showed a constitutional activation of the mRNA expression of the sensors of the three UPR arms *ERN1* (encoding IRE1α), *ATF6*, and *EIF2AK3* (encoding PERK). This was accompanied by a significant increase of the transcript levels of *HSPA5* encoding the chaperone BiP and of the downstream effectors *XBP1s* (IRE1α pathway) and *DDIT3* encoding CHOP (PERK pathway). However, analysis at the protein level did not demonstrate constitutional or induced activation of the UPR effectors IRE1, XBP1s, and CHOP (Figure S4).

Discussion

We provide here strong evidence that monoallelic pathogenic variants to *ALG5* underlie a nephropathy characterized by the development of small bilateral kidney cysts and renal interstitial fibrosis causing late-onset progressive loss of kidney function. *ALG5* had not been described in recessively inherited diseases, in contrast with other genes recently linked to atypical forms of polycystic kidney and/or liver disease, such as *PMM2, ALG8*, and *ALG9*, which were all initially described in congenital disorders of glycosylation (CDG), severe multisystemic diseases usually diagnosed prenatally or in infancy.[7,8,17,28]

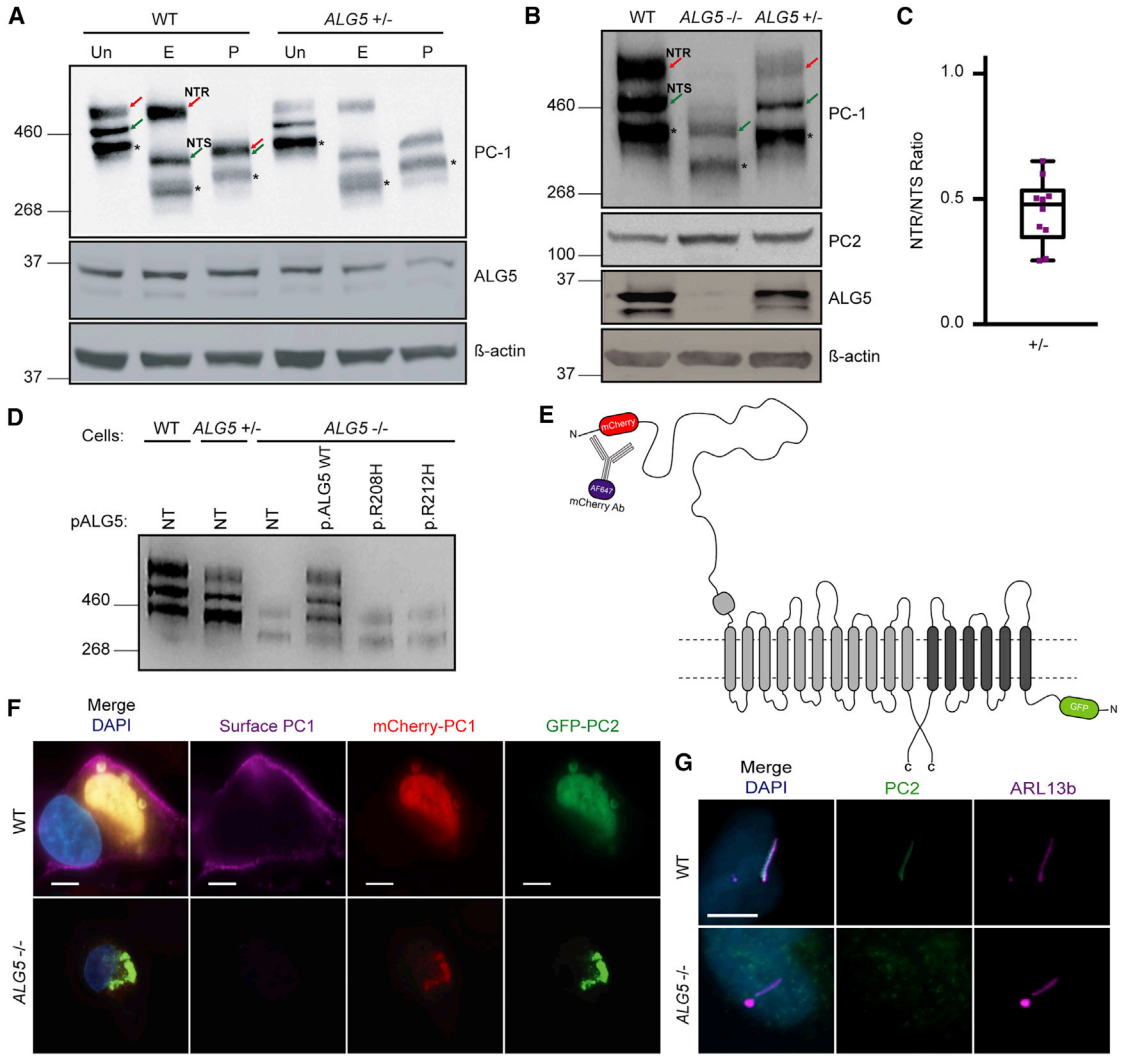

Figure 5. Characterization of the effect of *ALG5* loss on PC1 and PC2 abundance, maturation, and localization

(A) Western blot deglycosylation analysis of WT and $ALG5^{+/-}$ RCTE membrane protein either untreated (Un) or treated with EndoH (E) or PNGaseF (P). PC1 complex was immunodetected with the N-terminal PC1 (PC1-NT) antibody (7e12). Reduction of the mature PC1 glycoform (N-terminal, resistant to endoglycosidase H [PC1-NTR]) was observed in $ALG5^{-/+}$ cells. NTR (red arrow) indicates PC1-NTR, NTS (green arrow) indicates the immature form PC1-NTS (N-terminal PC1, sensitive to endoglycosidase H), * indicates Trunc-PC1, the protein product of abnormal differential splicing across introns 21 and 22 of *PKD1*.

(B) Western blot analysis of PC1 glycoforms in WT, $ALG5^{-/-}$ and $ALG5^{+/-}$ RCTE cells. PC1 was immunodetected with the N-terminal PC1 (PC1-NT) antibody (7e12). Complete loss of the mature PC1-NTR was observed in $ALG5^{-/-}$ cells. Altered migration of PC1-NTS is due to hypoglycosylation in $ALG5^{-/-}$ cells. In $ALG5^{+/-}$ cells, PC1-NTR level was reduced and the immature form PC1-NTS more abundant. PC2 protein level was increased in $ALG5^{-/-}$ cells. Loss of ALG5 was confirmed in $ALG5^{-/-}$ cells. NTR indicates PC1-NTR (red arrow), NTS indicates PC1-NTS (green arrow), * indicates Trunc_PC1.

(C) Quantification of PC1-NTR/NTS ratio shows a reduction to ~50% in heterozygous cells as compared to the WT RCTE cells. The PC1 NTR/NTS bands density were measured and normalized to WT results in 10 different experiments, and presented here as the mean, quartiles, and extreme values.

(D) Western blot showing that PC1 glycoform profile was rescued in $ALG5^{-/-}$ cells transfected with the WT pALG5 plasmid. Transfection with the identified *ALG5* missense variants cloned in pALG5, Arg208His, and Arg212His did not rescue PC1 maturation. NT, non transfected.

(E) Schematic representation of mCherry-PC1 and TagGFP-PC2 constructs.

(F) WT or $ALG5^{-/-}$ cells were co-transfected with WT tagged PC1 and PC2, mCherry-PC1, and TagGFP-PC2 and examined for surface PC1 labeling in co-transfected cells. Surface PC1 was detected in co-transfected WT cells but not in co-transfected $ALG5^{-/-}$ cells. Nuclei were stained with DAPI (in blue). The loss of PC1 membrane expression was confirmed in three independent experiments. Scale bar represents 10 μm.

(G) Primary cilia in WT and $ALG5^{-/-}$ cells in which ARL13B (ciliary marker) and PC2 were detected shows no cilia PC2 signal in $ALG5^{-/-}$ cells. Nuclei were stained with DAPI, and 50 ciliated cells were analyzed in three independent experiments. Scale bar represents 5 μm.

N-linked glycosylation of secretory and membrane proteins is an essential process that requires the biosynthesis and transfer of the oligosaccharide Glc3Man9GlcNAc2. ALG5 catalyzes the synthesis of the glucose-residue donor Dol-P-Glc, allowing the addition of the three glucose residues (Figure 1).[17] Previous data indicate that *ALG5*-null *S. cerevisiae* mutants do not exhibit any detectable growth defects, but are characterized by an under-glycosylation phenotype.[22] Data on a murine model indicate that the *Alg5* knockout is embryonically lethal.[29] In our study, analysis of the ER N-glycosylation pathway by metabolic labeling in renal epithelial cells showed a high rate of LLO transfer and maturation of the oligosaccharide species onto proteins, arguing that tubular epithelial cells have a high metabolic rate compared to other cell types.[24] Importantly, we show that *ALG5* haploinsufficiency is sufficient to alter the LLO synthesis as cells accumulate Man9GlcNAc2-PP-Dol species. We also demonstrated that lipid-linked Man9GlcNAc2 are transferred onto proteins leading to a delay in oligosaccharide maturation compared to WT cells, likely due to ER retention of misfolded N-glycoproteins. The apparent predominant kidney involvement might be explained by an increased vulnerability of renal epithelial cells to decreased levels of ALG5.

Seven genes involved in different steps of protein ER biogenesis had been previously associated to the ADPKD/ADPLD spectrum.[7–9,11,28,30,31] Pathogenic variants in these genes have been proven, or hypothesized, to result in a quantitative defect in mature PC1. *ALG5* follows this rule; importantly, we show that *ALG5* haploinsufficiency is associated with a significant decrease of the level of mature PC1. Detected PC2 N-glycosylation was not apparently affected by ALG5 loss. This is in accord with previous studies showing by whole membrane analysis that all detectable PC2 is sensitive to endoglycosidase H, suggesting that the large majority of PC2 is found in the ER.[32,33] While the molecular mechanism is not determined, a predominant posttranslational N-glycosylation process, mediated by the STT3B complex, could explain the absence of detectable underglycosylation of PC2. While defective PC1 maturation causes cystogenesis, the mechanisms underlying the development of interstitial fibrosis remains to be elucidated. Defective N-glycosylation likely affects other tubular proteins, increasing the load of misfolded protein in the ER. Our cellular studies show that *ALG5*-defective cells are characterized by increased transcription of the sensors and downstream effectors of the three UPR arms, although this was not confirmed at the protein level. The central role of UPR has been highlighted in ADTKD, in particular in ADTKD-*UMOD* where intracellular accumulation of mutant uromodulin causes ER stress and induction of UPR leading to a hyperinflammatory state and tubular cell death.[14,34,35] Similar pathogenic mechanisms might be involved in the development of progressive interstitial fibrosis in *ALG5* kidney disease.

The *ALG5* phenotype shows similarities with *DNAJB11* kidney disease, with late-onset development of CKD, atrophic kidneys, and multiple millimeter-sized kidney cysts.[10] While all individuals with *ALG5* pathogenic variants below 50 years of age had normal kidney functions, CKD was present in all affected individuals >60 years of age, and 8 individuals reached ESKD, with age at ESKD onset ranging from 62 to 91 years. The pathogenic mechanisms driving this seemingly accelerated decline of kidney function after the sixth decade remains elusive. *ALG5*-related kidney disease is a proteostasis disorder, and it is tempting to speculate that ALG5-depleted kidneys may have an increased susceptibility to aging, with epithelial tubular cells unable to cope with heavy loads of misfolded proteins increasing with age.[36,37] The occurrence of somatic second-hit mutations inactivating the normal copy of *ALG8* and *ALG9*, leading to a recessive genotype in individual cells, has been hypothesized to trigger cystogenesis in ADPLD caused by monoallelic mutations in these genes.[7,8] The *PKD1* locus is intrinsically prone to mutations due to the composition of its structure and sequence, and there is now a strong level of evidence to support the role of second-hit mutations at some stage in the pathogenesis of ADPKD-*PKD1* and *PKD2*.[38–41] Whether this second-hit mechanism also applies to the highly conserved *ALG* genes remains to our opinion uncertain.

None of the ALG5-affected individuals met the criteria for polycystic liver disease (≥10 liver cysts), and most of them did not have any detectable liver cysts. Although many ADPKD/ADPLD-affected families were screened for *ALG5* variants in this study, excluding the risk for clinically significant PLD in ALG5 disease will need the characterization of more families. The determinants of the kidney and or liver phenotypic predominance in this expanding group of glycosylation-associated cystic diseases is hitherto unresolved. Interestingly, colonic diverticulosis was reported in seven affected individuals from two families, and three of them underwent surgical procedures. While prevalence of diverticulosis in the general population is high (~30%–60%), symptomatic complicated disease is less frequent (~4% of those with diverticulosis).[42,43] Hirschprung's disease, a rare motor disorder of the gut presumably caused by a defective migration of neuroblasts during intestinal development, was reported in one ALG5-affected individual; partial colonic resection was performed in his first year of life. Because *ALG5* is ubiquitously expressed, we cannot exclude the possibility of additional extrarenal manifestations of the disease. Again, a larger number of *ALG5*-affected families are needed to distinguish coincidental clinical findings from *ALG5*-related phenotypes. The relatively low number of *ALG5*-affected families identified despite a very large genetic screening suggests that *ALG5*-associated nephropathy is an extremely rare disease. This is consistent with the prevalence of predicted pathogenic *ALG5* variants in the GnomAD database, with only 16 predicted loss-of-function variants identified in 141,456 individuals (1/8,841).[25] This may be partly explained by the relatively small size of the coding region. However, *ALG5* kidney disease is likely to be under-diagnosed, first because inherited kidney diseases are often not on the radar of physicians in individuals >60 years at disease

onset, and second because disease presentation remains largely nonspecific.[44,45] Determining the extent of *ALG5* pathogenic variants in people with unexplained or non-specific causes of CKD or ESKD, irrespective of their age, would be of interest.

Developing adequate and unified disease terminologies is an important goal in clinical genetics and in nephrogenetics.[15,46,47] Dyadic terminologies comprising both the clinical condition and the gene name have been suggested to provide flexibility for all users: researchers, clinicians, and patients.[48] The clinical and functional data presented herein establish *ALG5* as part of the ADPKD spectrum, and in agreement with recent publications, we suggest employing the term ADPKD-*ALG5*.[12] However, it is important to note that disease presentation, prognosis, and pathogenesis are distinct from ADPKD caused by pathogenic variants of *PKD1* and *PKD2*. In particular, imaging diagnosis criteria employed in ADPKD-*PKD1/PKD2* cannot be used in first-degree relatives of *ALG5*-affected individuals, who may not develop cysts before 50–60 years of age despite being affected.[48]

In conclusion, monoallelic pathogenic *ALG5* variants result in a fibrocystic disorder of the kidneys with progressive CKD. The identification of ADPKD-*ALG5* expands the family of glycosylation-associated kidney and liver diseases, with implications in diagnosis, genetic counselling, and prognosis evaluation, and may open the way to the development of specific therapeutic strategies.

Data and code availability

This study did not generate/analyze datasets and/or code

Supplemental information

Supplemental information can be found online at https://doi.org/10.1016/j.ajhg.2022.06.013.

Acknowledgments

We thank the families and coordinators for involvement in the study. The full list of investigators of the Genkyst Study is included in the supplemental data. We also thank Laila El Khattabi (Paris, France), Andrew Streets (Sheffield, UK), Nathalie Benz (UMR1078, Brest), and Nadège Marec and Jacques-Olivier Pers (Hyperion Platform, UMR1227 LBAI, Brest, France) for advice and/or technical assistance. We thank Mohamad Zaidan (APHP, Le Kremlin-Bicêtre) for patients' referral. The Mayo Clinic PKD Center is thanked for reagents used in this study.

The study was supported by National Research Agency grant (ANR JCJC 2019 GENOVAS-PKD, ECLG), a National Plan for Clinical Research (PHRC inter-regional GeneQuest, NCT02112136, ECLG), and a grant by the French Orphan Kidney diseases healthcare network (Filière maladies rares rénales ORKID 2020). E.O. is supported by the Swiss National Science Foundation (P2ZHP3_195181, P500PB_206851) and Kidney Research UK (Paed_RP_001_20180925). M.B.-G. is funded by Kidney Research UK (ST_001_20171120) and the Northern Counties Kidney Research Fund. F.F. is supported by the French National Agency (ANR-18-RAR3-0009-01) under the frame of E-Rare-3, the ERA-Net for Research on Rare Diseases (ERA-NET Cofund action no. 64578). J.A.S. is funded by Kidney Research UK and the Northern Counties Kidney Research Fund. B.K. and E.C.-L.G. are members of the European Reference Network for Rare Kidney Diseases (ERKNet), Project ID No 739532.

This research was made possible through access to the data and findings generated by the 100,000 Genomes Project (further information is detailed in the supplemental data, along with the full list of Genomics England investigators).

Declaration of interests

The authors declare no competing interests.

Received: March 11, 2022
Accepted: June 23, 2022
Published: July 26, 2022

Web resources

Addgene, https://www.addgene.org/

Combined Annotation Dependent Depletion, https://cadd.gs.washington.edu/

CRISPOR, http://crispor.tefor.net

GenBank, https://www.ncbi.nlm.nih.gov/genbank/

Genomics England 100K Project, https://www.genomicsengland.co.uk/

GnomAD Browser, https://gnomad.broadinstitute.org/

ImageJ, https://imagej.nih.gov/ij/

OMIM, http://www.omim.org

Renal Epidemiology and Information Network (REIN), annual report, rapport_rein_2019_2021-10-14.pdf (agence-biomedecine.fr)

Primer-BLAST, https://www.ncbi.nlm.nih.gov/tools/primer-blast/

UCSC Genome Browser, https://genome.ucsc.edu

United States Renal Data System, annual report, https://adr.usrds.org/2020

References

1. Cornec-Le Gall, E., Alam, A., and Perrone, R.D. (2019). Autosomal dominant polycystic kidney disease. Lancet *393*, 919–935. https://doi.org/10.1016/s0140-6736(18)32782-x.
2. Cornec-Le Gall, E., Torres, V.E., and Harris, P.C. (2018). Genetic complexity of autosomal dominant polycystic kidney and liver diseases. J. Am. Soc. Nephrol. : JASN *29*, 13–23. https://doi.org/10.1681/asn.2017050483.
3. Cornec-Le Gall, E., Audrézet, M.P., Rousseau, A., Hourmant, M., Renaudineau, E., Charasse, C., Morin, M.P., Moal, M.C., Dantal, J., Wehbe, B., et al. (2016). The PROPKD score: a new algorithm to predict renal survival in autosomal dominant polycystic kidney disease. J. Am. Soc. Nephrol. : JASN *27*, 942–951. https://doi.org/10.1681/asn.2015010016.
4. Ong, A.C.M., and Harris, P.C. (2015). A polycystin-centric view of cyst formation and disease: the polycystins revisited. Kidney Int. *88*, 699–710. https://doi.org/10.1038/ki.2015.207.
5. Hopp, K., Ward, C.J., Hommerding, C.J., Nasr, S.H., Tuan, H.-F., Gainullin, V.G., Rossetti, S., Torres, V.E., and Harris, P.C. (2012). Functional polycystin-1 dosage governs autosomal dominant

polycystic kidney disease severity. J. Clin. Invest. *122*, 4257–4273. https://doi.org/10.1172/jci64313.

6. Gainullin, V.G., Hopp, K., Ward, C.J., Hommerding, C.J., and Harris, P.C. (2015). Polycystin-1 maturation requires polycystin-2 in a dose-dependent manner. J. Clin. Invest. *125*, 607–620. https://doi.org/10.1172/jci76972.
7. Besse, W., Chang, A.R., Luo, J.Z., Triffo, W.J., Moore, B.S., Gulati, A., Hartzel, D.N., Mane, S., Regeneron Genetics, C., Somlo, S., et al. (2019). ALG9 mutation carriers develop kidney and liver cysts. J. Am. Soc. Nephrol. : JASN *30*, 2091–2102. https://doi.org/10.1681/asn.2019030298.
8. Besse, W., Dong, K., Choi, J., Punia, S., Fedeles, S.V., Choi, M., Gallagher, A.R., Huang, E.B., Gulati, A., Knight, J., et al. (2017). Isolated polycystic liver disease genes define effectors of polycystin-1 function. J. Clin. Invest. *127*, 3558. https://doi.org/10.1172/jci96729.
9. Cornec-Le Gall, E., Olson, R.J., Besse, W., Heyer, C.M., Gainullin, V.G., Smith, J.M., Audrézet, M.P., Hopp, K., Porath, B., Shi, B., et al. (2018). Monoallelic mutations to DNAJB11 cause atypical autosomal-dominant polycystic kidney disease. Am. J. Hum. Genet. *102*, 832–844. https://doi.org/10.1016/j.ajhg.2018.03.013.
10. Huynh, V.T., Audrézet, M.P., Sayer, J.A., Ong, A.C., Lefevre, S., Le Brun, V., Després, A., Senum, S.R., Chebib, F.T., Barroso-Gil, M., et al. (2020). Clinical spectrum, prognosis and estimated prevalence of DNAJB11-kidney disease. Kidney Int. *98*, 476–487. https://doi.org/10.1016/j.kint.2020.02.022.
11. Porath, B., Gainullin, V.G., Cornec-Le Gall, E., Dillinger, E.K., Heyer, C.M., Hopp, K., Edwards, M.E., Madsen, C.D., Mauritz, S.R., Banks, C.J., et al. (2016). Mutations in GANAB , encoding the glucosidase IIα subunit, cause autosomal-dominant polycystic kidney and liver disease. Am. J. Hum. Genet. *98*, 1193–1207. https://doi.org/10.1016/j.ajhg.2016.05.004.
12. Senum, S.R., Li, Y.S.M., Benson, K.A., Joli, G., Olinger, E., Lavu, S., Madsen, C.D., Gregory, A.V., Neatu, R., Kline, T.L., et al. (2022). Monoallelic IFT140 pathogenic variants are an important cause of the autosomal dominant polycystic kidney-spectrum phenotype. Am. J. Hum. Genet. *109*, 136–156. https://doi.org/10.1016/j.ajhg.2021.11.016.
13. Bergmann, C., Guay-Woodford, L.M., Harris, P.C., Horie, S., Peters, D.J.M., and Torres, V.E. (2018). Polycystic kidney disease. Nat. Rev. Dis. Primers *4*, 50. https://doi.org/10.1038/s41572-018-0047-y.
14. Devuyst, O., Olinger, E., Weber, S., Eckardt, K.U., Kmoch, S., Rampoldi, L., and Bleyer, A.J. (2019). Autosomal dominant tubulointerstitial kidney disease. Nat. Rev. Dis. Primers *5*, 60. https://doi.org/10.1038/s41572-019-0109-9.
15. Eckardt, K.U., Alper, S.L., Antignac, C., Bleyer, A.J., Chauveau, D., Dahan, K., Deltas, C., Hosking, A., Kmoch, S., Rampoldi, L., et al. (2015). Autosomal dominant tubulointerstitial kidney disease: diagnosis, classification, and management–A KDIGO consensus report. Kidney Int. *88*, 676–683. https://doi.org/10.1038/ki.2015.28.
16. Heyer, C.M., Sundsbak, J.L., Abebe, K.Z., Chapman, A.B., Torres, V.E., Grantham, J.J., Bae, K.T., Schrier, R.W., Perrone, R.D., Braun, W.E., et al. (2016). Predicted mutation strength of nontruncating PKD1 mutations aids genotype-phenotype correlations in autosomal dominant polycystic kidney disease. J. Am. Soc. Nephrol. : JASN *27*, 2872–2884. https://doi.org/10.1681/asn.2015050583.
17. Schjoldager, K.T., Narimatsu, Y., Joshi, H.J., and Clausen, H. (2020). Global view of human protein glycosylation pathways and functions. Nat. Rev. Mol. Cel. Biol. *21*, 729–749. https://doi.org/10.1038/s41580-020-00294-x.
18. Hughes, J., Ward, C.J., Peral, B., Aspinwall, R., Clark, K., San Millán, J.L., Gamble, V., and Harris, P.C. (1995). The polycystic kidney disease 1 (PKD1) gene encodes a novel protein with multiple cell recognition domains. Nat. Genet. *10*, 151–160. https://doi.org/10.1038/ng0695-151.
19. Hofherr, A., Wagner, C., Fedeles, S., Somlo, S., and Köttgen, M. (2014). N-glycosylation determines the abundance of the transient receptor potential channel TRPP2. J. Biol. Chem. *289*, 14854–14867. https://doi.org/10.1074/jbc.m114.562264.
20. Helenius, A., and Aebi, M. (2004). Roles of N-linked glycans in the endoplasmic reticulum. Annu. Rev. Biochem. *73*, 1019–1049. https://doi.org/10.1146/annurev.biochem.73.011303.073752.
21. Imbach, T., Burda, P., Kuhnert, P., Wevers, R.A., Aebi, M., Berger, E.G., and Hennet, T. (1999). A mutation in the human ortholog of the Saccharomyces cerevisiae ALG6 gene causes carbohydrate-deficient glycoprotein syndrome type-Ic. Proc. Natl. Acad. Sci. USA *96*, 6982–6987. https://doi.org/10.1073/pnas.96.12.6982.
22. Heesen, S.T., Lehle, L., Weissmann, A., and Aebi, M. (1994). Isolation of the ALG5 locus encoding the UDP-glucose:dolichyl-phosphate glucosyltransferase from Saccharomyces cerevisiae. Eur. J. Biochem. *224*, 71–79. https://doi.org/10.1111/j.1432-1033.1994.tb19996.x.
23. Levey, A.S., Stevens, L.A., Schmid, C.H., Zhang, Y.L., Castro, A.F., 3rd, Feldman, H.I., Kusek, J.W., Eggers, P., Van Lente, F., Greene, T., and Coresh, J. (2009). A new equation to estimate glomerular filtration rate. Ann. Intern. Med. *150*, 604. https://doi.org/10.7326/0003-4819-150-9-200905050-00006.
24. Péanne, R., Vanbeselaere, J., Vicogne, D., Mir, A.M., Biot, C., Matthijs, G., Guérardel, Y., and Foulquier, F. (2013). Assessing ER and Golgi N-glycosylation process using metabolic labeling in mammalian cultured cells. Methods Cell Biol. *118*, 157–176. https://doi.org/10.1016/B978-0-12-417164-0.00010-0.
25. Karczewski, K.J., Francioli, L.C., Tiao, G., Cummings, B.B., Alföldi, J., Wang, Q., Collins, R.L., Laricchia, K.M., Ganna, A., Birnbaum, D.P., et al. (2020). The mutational constraint spectrum quantified from variation in 141, 456 humans. Nature *581*, 434–443. https://doi.org/10.1038/s41586-020-2308-7.
26. Lea, W.A., Parnell, S.C., Wallace, D.P., Calvet, J.P., Zelenchuk, L.V., Alvarez, N.S., and Ward, C.J. (2018). Human-specific abnormal alternative splicing of wild-type PKD1 induces premature termination of polycystin-1. J. Am. Soc. Nephrol. : JASN *29*, 2482–2492. https://doi.org/10.1681/asn.2018040442.
27. Kim, H., Xu, H., Yao, Q., Li, W., Huang, Q., Outeda, P., Cebotaru, V., Chiaravalli, M., Boletta, A., Piontek, K., et al. (2014). Ciliary membrane proteins traffic through the Golgi via a Rabep1/GGA1/Arl3-dependent mechanism. Nat. Commun. *5*, 5482. https://doi.org/10.1038/ncomms6482.
28. Cabezas, O.R., Flanagan, S.E., Stanescu, H., García-Martínez, E., Caswell, R., Lango-Allen, H., Antón-Gamero, M., Argente, J., Bussell, A.M., Brandli, A., et al. (2017). Polycystic kidney disease with hyperinsulinemic hypoglycemia caused by a promoter mutation in phosphomannomutase 2. J. Am. Soc. Nephrol. : JASN *28*, 2529–2539. https://doi.org/10.1681/asn.2016121312.
29. García-García, M.J., Eggenschwiler, J.T., Caspary, T., Alcorn, H.L., Wyler, M.R., Huangfu, D., Rakeman, A.S., Lee, J.D., Feinberg, E.H., Timmer, J.R., and Anderson, K.V. (2005). Analysis of mouse embryonic patterning and morphogenesis by

forward genetics. Proc. Natl. Acad. Sci. USA *102*, 5913–5919. https://doi.org/10.1073/pnas.0501071102.

30. Davila, S., Furu, L., Gharavi, A.G., Tian, X., Onoe, T., Qian, Q., Li, A., Cai, Y., Kamath, P.S., King, B.F., et al. (2004). Mutations in SEC63 cause autosomal dominant polycystic liver disease. Nat. Genet. *36*, 575–577. https://doi.org/10.1038/ng1357.
31. Drenth, J.P., te Morsche, R.H., Smink, R., Bonifacino, J.S., and Jansen, J.B. (2003). Germline mutations in PRKCSH are associated with autosomal dominant polycystic liver disease. Nat. Genet. *33*, 345–347. https://doi.org/10.1038/ng1104.
32. Newby, L.J., Streets, A.J., Zhao, Y., Harris, P.C., Ward, C.J., and Ong, A.C. (2002). Identification, characterization, and localization of a novel kidney polycystin-1-polycystin-2 complex. J. Biol. Chem. *277*, 20763–20773. https://doi.org/10.1074/jbc.m107788200.
33. Cai, Y., Maeda, Y., Cedzich, A., Torres, V.E., Wu, G., Hayashi, T., Mochizuki, T., Park, J.H., Witzgall, R., and Somlo, S. (1999). Identification and characterization of polycystin-2, the PKD2 gene product. J. Biol. Chem. *274*, 28557–28565. https://doi.org/10.1074/jbc.274.40.28557.
34. Johnson, B.G., Dang, L.T., Marsh, G., Roach, A.M., Levine, Z.G., Monti, A., Reyon, D., Feigenbaum, L., and Duffield, J.S. (2017). Uromodulin p.Cys147Trp mutation drives kidney disease by activating ER stress and apoptosis. J. Clin. Invest. *127*, 3954–3969. https://doi.org/10.1172/jci93817.
35. Schaeffer, C., Merella, S., Pasqualetto, E., Lazarevic, D., and Rampoldi, L. (2017). Mutant uromodulin expression leads to altered homeostasis of the endoplasmic reticulum and activates the unfolded protein response. PLoS ONE *12*, e0175970. https://doi.org/10.1371/journal.pone.0175970.
36. Hipp, M.S., Kasturi, P., and Hartl, F.U. (2019). The proteostasis network and its decline in ageing. Nat. Rev. Mol. Cell Biol. *20*, 421–435. https://doi.org/10.1038/s41580-019-0101-y.
37. Inagi, R., Ishimoto, Y., and Nangaku, M. (2014). Proteostasis in endoplasmic reticulum–new mechanisms in kidney disease. Nat. Rev. Nephrol. *10*, 369–378. https://doi.org/10.1038/nrneph.2014.67.
38. Tan, A.Y., Zhang, T., Michaeel, A., Blumenfeld, J., Liu, G., Zhang, W., Zhang, Z., Zhu, Y., Rennert, L., Martin, C., et al. (2018). Somatic mutations in renal cyst epithelium in autosomal dominant polycystic kidney disease. J. Am. Soc. Nephrol. : JASN *29*, 2139–2156. https://doi.org/10.1681/asn.2017080878.
39. Zhang, Z., Bai, H., Blumenfeld, J., Ramnauth, A.B., Barash, I., Prince, M., Tan, A.Y., Michaeel, A., Liu, G., Chicos, I., et al. (2021). Detection of PKD1 and PKD2 somatic variants in autosomal dominant polycystic kidney cyst epithelial cells by whole-genome sequencing. J. Am. Soc. Nephrol. : JASN *32*, 3114–3129. https://doi.org/10.1681/asn.2021050690.
40. Qian, F., Watnick, T.J., Onuchic, L.F., and Germino, G.G. (1996). The molecular basis of focal cyst formation in human autosomal dominant polycystic kidney disease type I. Cell *87*, 979–987. https://doi.org/10.1016/s0092-8674(00)81793-6.
41. Watnick, T.J., Torres, V.E., Gandolph, M.A., Qian, F., Onuchic, L.F., Klinger, K.W., Landes, G., and Germino, G.G. (1998). Somatic mutation in individual liver cysts supports a two-hit model of cystogenesis in autosomal dominant polycystic kidney disease. Mol. Cell *2*, 247–251. https://doi.org/10.1016/s1097-2765(00)80135-5.
42. Tursi, A., Scarpignato, C., Strate, L.L., Lanas, A., Kruis, W., Lahat, A., and Danese, S. (2020). Colonic diverticular disease. Nat. Rev. Dis. Primers *6*, 20. https://doi.org/10.1038/s41572-020-0153-5.
43. Shahedi, K., Fuller, G., Bolus, R., Cohen, E., Vu, M., Shah, R., Agarwal, N., Kaneshiro, M., Atia, M., Sheen, V., et al. (2013). Long-term risk of acute diverticulitis among patients with incidental diverticulosis found during colonoscopy. Clin. Gastroenterol. Hepatol. *11*, 1609–1613. https://doi.org/10.1016/j.cgh.2013.06.020.
44. Knoers, N., Antignac, C., Bergmann, C., Dahan, K., Giglio, S., Heidet, L., Lipska-Ziętkiewicz, B.S., Noris, M., Remuzzi, G., Vargas-Poussou, R., et al. (2021). Genetic testing in the diagnosis of chronic kidney disease: recommendations for clinical practice. Nephrology, Dialysis, Transplantation *37*, 239–254.
45. Cornec-Le Gall, E., and Harris, P.C. (2018). The underestimated burden of monogenic diseases in adult-onset ESRD. J. Am. Soc. Nephrol. : JASN *29*, 1583–1584. https://doi.org/10.1681/asn.2018040441.
46. Biesecker, L.G., Adam, M.P., Alkuraya, F.S., Amemiya, A.R., Bamshad, M.J., Beck, A.E., Bennett, J.T., Bird, L.M., Carey, J.C., Chung, B., et al. (2021). A dyadic approach to the delineation of diagnostic entities in clinical genomics. Am. J. Hum. Genet. *108*, 8–15. https://doi.org/10.1016/j.ajhg.2020.11.013.
47. Kashtan, C.E., Ding, J., Garosi, G., Heidet, L., Massella, L., Nakanishi, K., Nozu, K., Renieri, A., Rheault, M., Wang, F., and Gross, O. (2018). Alport syndrome: a unified classification of genetic disorders of collagen IV α345: a position paper of the Alport Syndrome Classification Working Group. Kidney Int. *93*, 1045–1051. https://doi.org/10.1016/j.kint.2017.12.018.
48. KDIGO conference participants (2022). Genetics in chronic kidney disease: conclusions from a kidney disease: improving global outcomes (KDIGO) controversies conference. Kidney Int. *101*, 1126–1141.